JOURNAL OF PETROLOGY | VOLUME 43 | NUMBER 5 | PAGES 749–768 | 2002

Kinetic Controls on the Partitioning of Trace Elements Between Silicate and Sulfide Liquids

J. E. MUNGALL*

DEPARTMENT OF GEOLOGY, UNIVERSITY OF TORONTO, 22 RUSSELL STREET, TORONTO, ONT., M5S 3B1, CANADA

RECEIVED MARCH 12, 2001; REVISED TYPESCRIPT ACCEPTED NOVEMBER 8, 2001

Mass transfer between sulfide and silicate liquids is often discussed by reference to a mass ratio between hypothetical liquid reservoirs at equilibrium, defined as R. *In an open system not at equilibrium the mass of silicate melt from which a growing sulfide droplet appears to have scavenged chalcophile elements will depend on diffusivities* D_i *and* D_{FeS} *of the element and of the FeS component in the silicate melt, respectively, on the degree of supersaturation of the melt with FeS* C_o^{FeS}, *on the radius* a *of the droplet and on the velocity* v *with which the droplet is advected through the melt, so that*

$$R = \frac{1}{C_o^{FeS}}\left(\frac{D_i + 1/2\sqrt{aD_iv}}{D_{FeS} + 1/2\sqrt{aD_{FeS}v}}\right).$$

Chalcophile elements are expected to show inter-element variations in D *spanning several orders of magnitude in some melts, leading to large inter-element variations in effective* R *in a given sulfide body. These variations in effective* R *will lead to spatial separations between zones of maximum enrichment of chalcophile elements produced during fractional segregation of sulfide in layered intrusions. Whereas it has proven impossible to model the generation of spatially offset stratiform horizons in the Australian Munni Munni layered intrusion using equilibrium partition coefficients, the present kinetic model reproduces the observed patterns with great fidelity.*

KEY WORDS: *chalcophile element; platinum group element; partitioning; sulfide melt; silicate melt; R factor*

INTRODUCTION

The formation of many magmatic Ni–Cu–Co deposits, which may contain significant accessory platinum group elements (PGE), has resulted from liquation (immiscible liquid phase separation) of sulfide liquid from mafic or ultramafic silicate magma. A central assumption of models of magmatic sulfide deposit formation is that the base metals and PGE are strongly partitioned into the sulfide melt. Previous discussions of the process by which sulfide liquids become enriched in chalcophile metals have focused almost exclusively on models in which coexisting bodies of sulfide and silicate melt are considered to be in equilibrium at all times.

The intent of this paper is to demonstrate that natural sulfide deposits preserved in igneous rocks will in many instances record metal distributions that never attained equilibrium, as a result of the kinetic constraints on metal partitioning between phases. The consequences are that different elements will seem to show evidence for equilibration at different silicate/sulfide mass ratios within single sulfide bodies. I describe the time-dependent evolution of metal distributions in silicate–sulfide melt systems, starting with analytical solutions for simple boundary conditions and then adapting them to more complex systems as numerical models.

Equilibrium partitioning of metals

The idea that the ratio between the masses of interacting silicate and sulfide magmas, defined as *R*, could have a profound impact on the type and grade of mineralization produced during and after a sulfide liquation event was introduced by Campbell & Naldrett (1979). Most subsequent studies of magmatic sulfide deposits have included this concept as an essential part of their ore deposit

*Telephone: 416 978 2975. Fax: 416 978 3938.
E-mail: mungall@geology.utoronto.ca

Table 1: Notation

Symbol	Definition	Units
C_{sil}	concentration in silicate melt	—
C_{sul}	concentration in sulfide melt	—
$C_{(r,t)}$	concentration at radius r and time t	—
C_o	concentration in the far-field or initial bulk concentration	—
C_s	concentration in silicate at the sulfide–silicate interface	—
C_o^{FeS}	difference between FeS concentration and its equilibrium concentration	—
K_D	sulfide–silicate partition coefficient	—
R	ratio of the mass of silicate to the mass of sulfide	—
η	dynamic viscosity	Pa s
D_i, D_j	diffusion coefficients of elements i, j in silicate melt	$cm^2\ s^{-1}$
D_{FeS}	diffusion coefficient of FeS in silicate melt	$cm^2\ s^{-1}$
ρ_{sil}	density of silicate melt	$g\ cm^{-3}$
ρ_{sul}	density of sulfide melt	$g\ cm^{-3}$
$\Delta\rho$	difference in density between sulfide and silicate melt	$g\ cm^{-3}$
g	acceleration due to gravity	$cm\ s^{-2}$
t	time	s
v	velocity	$cm\ s^{-1}$
a	length scale of a sulfide body (e.g. radius)	cm
r	distance from the center of the radial coordinate system	cm
x	distance from the origin of a one-dimensional system	cm
y	distance along a planar sheet	cm
X	downstream extent of a planar sheet of sulfide	cm
A	surface area of a sulfide body	cm^2
V	volume of a sulfide body	cm^3
M	time-integrated flux	$g\ cm^{-2}$
L	characteristic length	cm
m	mass transfer coefficient	$g\ cm^{-2}\ s^{-1}$
J	flux through a silicate–sulfide interface	$g\ cm^{-2}\ s^{-1}$

models. The starting point of the discussion of the R factor is the Nernst partition coefficient K_D, which is defined as

$$K_D = \frac{C_{sul}}{C_{sil}} \quad (1)$$

where C_{sul} is the concentration of a minor or trace element in the sulfide melt and C_{sil} its concentration in the coexisting silicate liquid if the two melts are allowed to reach equilibrium. Notation for this paper is summarized for easy reference in Table 1. In a closed system the total amount of the metal in question is fixed, and the consequent mass balance constraint leads to the following relation (Campbell & Naldrett, 1979):

$$\frac{C_{sul}}{C_o} = K_D \frac{(1 + R)}{(K_D + R)} \quad (2)$$

where C_o is the concentration of the element in the bulk system. For PGE, K_D of the order of 50 000 (e.g. Fleet *et al.*, 1999) and initial concentrations in the melt of 1–10 ppb permit concentrations up to 100 ppm in sulfide liquids. Rocks containing disseminated PGE-rich sulfide can thus attain bulk concentrations of PGE of the order of tens of ppm and as such can constitute important ores of the PGE. Actual concentrations of metals in coexisting sulfide ores and silicate rocks measured in real systems suggest that R factors of the order of 100–500 may have prevailed in the formation of the Ni-rich massive sulfides at Kambalda (Lesher & Campbell, 1993). The large Ni–Cu deposits of the Noril'sk camp may have been formed at R values of the order of 1000 (Brugman *et al.*, 1993), whereas R factors as high as 100 000 have been suggested for the PGE-enriched sulfide melts in the Merensky reef of the Bushveld Intrusive Complex (e.g. Campbell *et al.*, 1984).

KINETIC CONTROLS ON METAL PARTITIONING

Background

The previous discussion of metal partitioning between coexisting silicate and sulfide melts has assumed that they interact within a closed system at equilibrium, despite the fact that ore-forming magmatic systems are complex open systems. In natural systems metal partitioning occurs between droplets or pools of sulfide melt and moving bodies of silicate magma, much of which subsequently departs from the local system. To account for the large R factors inferred for some ore deposits, it is necessary to postulate that the sulfide liquid has passed through or been bypassed by great quantities of silicate magma (e.g. Naldrett *et al.*, 1992).

Previous discussions of kinetic controls on metal partitioning have been restricted in their scope. Barnes (1993) devoted a paragraph to kinetic considerations but confined his discussion to the effects of K_D on the size of a diffusive boundary layer. He indicated that apparent R values will be smaller for elements with larger K_D, but did not make any explicit comment on the role that different diffusivities might play in controlling metal partitioning. Barnes (1998) observed that metal ratios among the chalcophile elements commonly differ between ores and their inferred silicate parents for metals with similar equilibrium partitioning coefficients. She suggested, among other possibilities, that fast-diffusing metals may move more efficiently into sulfide droplets, leading to higher R factors for the more mobile elements.

Lesher & Campbell (1993) suggested that small droplets suspended in turbulently convecting silicate magma would scavenge metals more efficiently than would large drops or pools of sulfide melt.

Formulation of the problem

Disequilibrium between coexisting sulfide and silicate liquids causes chemical diffusion of melt components tending to bring the two phases into the equilibrium compositions described by equation (1). Elements with high diffusivities D will be able to move toward the silicate–sulfide interface faster than slowly diffusing elements. The more mobile elements will thus appear to have been gathered into the sulfide melt from larger volumes of silicate melt, and assessment of the relative concentrations of two different elements in the coexisting phases will lead to conflicting estimates of the effective ratio R between silicate and sulfide liquids that have interacted.

Throughout the following discussion, I assume that the sulfide melt is effectively inviscid and well mixed. Furthermore, I initially restrict the discussion to those situations in which the far-field concentration of a metal in the silicate melt C_o is much greater than its concentration at the interface with the sulfide melt C_s, so that C_s may be considered to be effectively constant. In reality, the metal content of the sulfide melt will increase with time, so that the concentration of the metal in the silicate melt at the interface will also rise as a result of the constraint imposed by equation (1). If C_s increases until $C_s > \sim 0{\cdot}1\ C_o$ then the assumption of constant C_s is no longer valid. By reference to equation (2), and assuming that $R \gg 1$, one can see that this situation will arise whenever $10R > K_D$, i.e. whenever R attains a value about one order of magnitude smaller than K_D. The more geologically interesting situation in which the magnitude of R approaches or exceeds K_D will be treated numerically after the derivation of the analytical expressions.

Static systems

One can consider two idealized geometries in which silicate and sulfide liquids might interact. At one extreme, the sulfide melt forms small droplets that are suspended in the silicate melt. If the droplets are small enough, they will sink through the silicate melt at a negligible rate, and their interaction with the silicate magma will result entirely from diffusive mass transfer free from the effects of advection in the silicate melt. The silicate melt surrounding each droplet may be modeled as an infinite space containing a spherical cavity. Alternatively, to address the effect of limited volumes of silicate melt (finite R factor) the system can be modeled as a spherical shell of silicate melt surrounding the droplet, with a zero-flux condition at the outside of the droplet.

At the other extreme, the sulfide liquid may collect into a large pool, which, because of its greater density, will sit in a depression at the base of a silicate magma chamber or conduit. In this case, the sulfide melt may be considered to be an infinite sheet below a planar interface adjacent to a silicate melt body forming a half-space. If the silicate melt is at rest then the mass transfer is entirely diffusive, and can be treated as a one-dimensional flux from a half-space into a sheet.

Given the assumption that mass transfer within the sulfide liquid is instantaneous (i.e. it is well mixed), only diffusion within the silicate melt needs to be considered. The derivations of equations governing mass transfer in the two static systems described above are given in the Appendix.

The addition of an advective term to any diffusive mass transfer problem will introduce an additional term with a linear time dependence, speeding the process at long time scales. Solutions to heat transfer problems can provide exact analogies to mass transfer problems through simple linear transformations. In the Appendix, I apply models of convective and conductive heat transfer (Pitts

& Sissom, 1977; Marsh, 1982) to the convected cases of the static problems above by defining expressions for coefficients of mass transfer and relating them to fluxes and effective R factors.

Analytical expressions for mass transfer

Equations (A5), (A8), (A16), (A22) and (A23) give the amount M (in g cm^{-2}) of metal that will have passed through a unit area of interface in a given time for the five geometries considered. The concentration of the metal in the sulfide liquid is related to M, the surface area A of the sulfide body, the volume V and density ρ_{sul} of the sulfide:

$$C_{sul} = \frac{MA}{\rho_{sul} V}. \quad (3)$$

The resulting variation of C_{sul} with time for a variety of geometries is given below:
static spherical droplet:

$$C_{sul} = 3\,\frac{\rho_{sil}}{\rho_{sul}}(C_o - C_s)\left(\frac{Dt}{a^2} + \sqrt{\frac{4Dt}{\pi a^2}}\right) \quad (4)$$

static planar interface:

$$C_{sul} = \frac{2}{\sqrt{\pi}}\,\frac{\rho_{sil}}{\rho_{sul}}(C_o - C_s)\sqrt{\frac{Dt}{a^2}} \quad (5)$$

moving silicate melt above a planar interface:

$$C_{sul} = \frac{3\sqrt{2}}{4}\,\frac{\rho_{sil}}{\rho_{sul}}(C_o - C_s)\sqrt{\frac{Dt}{a^2}}\cdot\sqrt{\frac{vt}{X}} \quad (6)$$

spherical droplet falling through static silicate melt:

$$C_{sul} = 3\,\frac{\rho_{sil}}{\rho_{sul}}(C_o - C_s)\left(\frac{Dt}{a^2} + \sqrt{\frac{Dt}{a^2}}\cdot\sqrt{\frac{vt}{4a}}\right) \quad (7)$$

spherical droplet in an external flow:

$$C_{sul} = 3\,\frac{\rho_{sil}}{\rho_{sul}}(C_o - C_s)\left(\frac{Dt}{a^2} + \sqrt{\frac{Dt}{a^2}}\cdot\sqrt{\frac{vt}{4L}}\right) \quad (8)$$

where C_{sul}, C_o and C_s are the metal concentrations in the sulfide melt, and in the silicate melt in the far field and at the interface, respectively; ρ_{sil} and ρ_{sul} are the densities of the silicate and sulfide melts, D is the diffusivity of the metal in silicate melt, t is time, a is a characteristic length scale (radius of droplet or depth of sulfide pool), v is the velocity of a flow, L is the length scale of an external flow and X is the downstream extent of a sulfide pool.

All of equations (4)–(8) contain the dimensionless term

$$\frac{\rho_{sil}}{\rho_{sul}}(C_o - C_s)$$

which scales the results to the melt densities and metal concentrations present. Time dependence of mass transfer into sulfide is scaled to diffusivity and the dimensions of the sulfide body through the dimensionless terms,

$$\sqrt{\frac{Dt}{a^2}},\ \frac{Dt}{a^2},\ \text{and}\ \sqrt{\frac{vt}{a}}\ \text{or}\ \sqrt{\frac{vt}{L}}.$$

To those readers familiar with problems involving diffusion in static systems the presence of a linear time dependence in the static case represented by equation (4) will appear remarkable. The reason it appears is that the temporal reduction in supply of solute to the interface as a result of lessening of the concentration gradient at the interface is exactly balanced by the focusing of solute from an increasingly large volume into the interface region.

The forms of equations (4)–(8) all show explicit dependences on the diffusion coefficient D of the metal under consideration. Whereas the two solutions for the planar interface show square-root dependences on D, the three solutions for spherical sulfide drops share a linear dependence on D. Diffusion coefficients for metals in silicate melts vary strongly with temperature, melt composition, and with the characteristics (charge, ionic radius) of the cations themselves (e.g. Henderson *et al.*, 1985; Mungall, 2002*a*). Differences in charge and ionic radius can induce inter-metal variations in D of up to four orders of magnitude in some melts. There is therefore a potential for mass fluxes to differ by four orders of magnitude for two different metals into the same sulfide droplet. This is a first-order effect that cannot safely be ignored in treatments of silicate–sulfide mass ratios.

Estimation of *R* factors

To calculate a mass of silicate melt m_{sil} from which the metal would have been extracted had the process actually been an equilibrium partitioning event, the mass of metal added to the droplet must be divided by the difference between the initial concentration of the metal in the silicate melt and concentration C_s it would have in the silicate melt at equilibrium with the sulfide droplet after the mass transfer had taken place:

$$m_{sil} = \frac{C_{sul}\, V_{sul}\, \rho_{sul}}{C_o - C_s}. \quad (9)$$

Comparing this hypothetical mass of equilibrated silicate melt with the mass of the sulfide body and simplifying we find

$$R = \frac{C_{sul}\, K_D}{C_o\, K_D - C_{sul}}. \quad (10)$$

An identical result is obtained from equation (2) if $R \gg K_D$, which is tantamount to neglecting the mass of the sulfide melt body within the mass of the entire system. However, equation (10) describes an apparent R factor that would be calculated for a single metal in a sulfide melt that has not reached equilibrium with its silicate host, whereas R in equation (2) describes a true ratio between the masses of two discrete and fully equilibrated melt reservoirs.

At short times, before C_{sul} approaches the magnitude of C_oK_D, equation (10) simplifies to

$$R = \frac{C_{sul}}{C_{sil}} \quad (11)$$

so that equations (4)–(8) give the effective R factor when simply divided by C_{sil}.

Numerical models

The dependence of R on time that can be obtained by combining equation (11) with any one of equations (4)–(8) is applicable only at short times before the composition of the sulfide reservoir has been significantly affected, as discussed in the formulation of the problem above. To estimate R at longer times it is necessary to resort to numerical methods, using the full form of equation (10) and allowing C_{sul} to vary according to the results of one of equations (4)–(8) in a sequence of discrete time steps. Each time step begins with C_o equal to the original far-field concentration, but with C_s reset to be in equilibrium with the value of C_{sul} calculated in the previous time step, by applying equation (1). The key concept behind this approach is the assumption that the rate of increase of C_{sul} is slow compared with the rate at which the near-field diffusion profile will be established. As long as this is true, a series of discrete steps can be modeled, each as a steady-state system as per the assumptions behind the derivations of the flux equations in the Appendix, with the initial conditions for each time step having been set by the final conditions of the previous step. That this should not introduce significant instabilities in the numerical simulations is supported by the coincidence of the analytical and numerical solutions for the static sphere shown in Fig. 1. Values for the other parameters in equations (4)–(8) have been varied in the following section to cover their plausible ranges.

Equation (11) shows that if a pre-existing sulfide drop of finite size is introduced to a silicate melt, the partition coefficient of a chalcophile element does not play any direct role in the composition of the sulfide droplet until metal concentrations in the silicate melt at the interface approach those of the far-field concentration. All behavior at relatively short times is controlled by kinetics, and the equilibrium partition coefficient is relevant only after much of the mass transfer has already taken place.

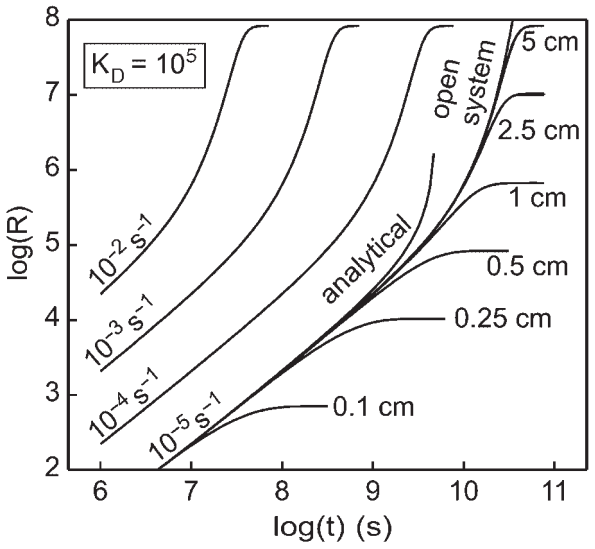

Fig. 1. Log R factor vs log time at constant K_D, static case. Each curve shows results for the indicated value of D/a^2, at a constant $K_D = 10^5$. (See text for explanation.)

Figure 1 is a logarithmic plot of the apparent R factor vs t for the case of the static spherical sulfide droplet when $D/a^2 = 10^{-2}$ (consider that a value of $D/a^2 = 10^{-2}$ s^{-1} could correspond to a diffusivity of 10^{-6} cm^2 s^{-1}, near the upper limit of diffusivities observed in silicate melts, and a droplet radius of 0·01 cm). The curve labelled 'open system' was calculated using equation (4) in a series of finite time steps as described above. Also shown in Fig. 1 is the curve calculated using the analytical expression for R obtained by combining equations (4) and (11).

The analytical solution is equivalent to the numerical model at times when $C_{sul} \ll C_oK_D$. As C_{sul} approaches C_oK_D the analytical solution begins to increase rapidly, and encounters a singularity at the time when C_s equals C_o. This behavior results from the incorrect assumption of constant $C_s = 0$ that went into the derivation of the analytical expressions. The numerical model shows the same initial linear increase of effective R against time until the metal concentration in the sulfide begins to rise significantly. Although the slope begins to increase here also, no singularity is reached because in the numerical model the metal flux into the sulfide diminishes as the metal concentration in the sulfide rises.

If two metals are characterized by different diffusivities D_i and D_j, their effective R factors at any given time will

differ by a factor of at least D_i/D_j. Because of the change in slope shown in Fig. 1, effective R factors may differ by as much as an additional factor of 100 during the time when the concentration of the faster diffusing metal has already begun its steep rise but the slower one remains on the linear portion of the curve. It is important to recall that if R greatly exceeds K_D the metal concentration becomes sensibly constant at the equilibrium value predicted by equation (1).

To test the validity of the numerical approach I have implemented an implicit finite-difference scheme (Crank, 1975) to calculate model diffusion profiles around a droplet in a static spherical shell of silicate melt. The boundary condition at the inner radius of the spherical shell of silicate melt is the concentration that would be in equilibrium with the metal concentration calculated for the sulfide droplet in the previous time step, whereas the outer radius of the spherical shell is subjected to a no-flux condition. The diffusion profile is integrated over the spherical diffusion region and used to calculate a mass uptake of metal by the droplet, which allows the new metal concentration within the drop to be calculated. The new metal concentration is used to update the boundary condition on the inner surface of the spherical shell for the next time step. As the implicit finite-difference scheme is stable, it provides a useful check on the accuracy of the other numerical model. The implicit finite difference model can also be used to investigate the effects of competition between droplets for metals, by varying the outer radius of the spherical shell of silicate melt to establish different silicate/sulfide mass ratios. The presence of a finite volume of silicate melt leads to the eventual establishment of a fully equilibrated silicate–sulfide melt system in which concentration gradients have been erased by diffusion and the system has attained an equilibrium closed system R factor equal for all metals present.

The results of a series of runs of the implicit finite difference model for the same conditions as the analytical and numerical model curves with indicated choices of D/a^2 are also shown in Fig. 1, as curves flattening off to constant (equilibrium) values of R at long times. Each curve with $D/a^2 = 10^{-5}$ is labelled with the diameter of the outer shell employed in the simulation; another series of curves with different values of D/a^2 form a series of parallel trends offset to higher R values. Small outer shell radii correspond to smaller R values of the bulk system; the choice of $D/a^2 = 10^{-5}$ was made to demonstrate the equivalence of the numerical models to values of R much larger than are usually thought to obtain in natural systems.

It is worth pointing out here that, as the time scale is logarithmic, the relative importance of times at the right-hand side of Fig. 1 is much greater than the earlier times. For example, the time between 10^6 and 10^8 s, during which the curves labelled $D/a^2 = 10^{-2}$ and $D/a^2 = 10^{-3}$ diverge by an additional order of magnitude, represents a period of about 3 years, whereas the entire initial period during which the two curves remained parallel lasted only for 1 month. After about 10 years the two curves converge on the equilibrium value of R of $\sim 10^8$.

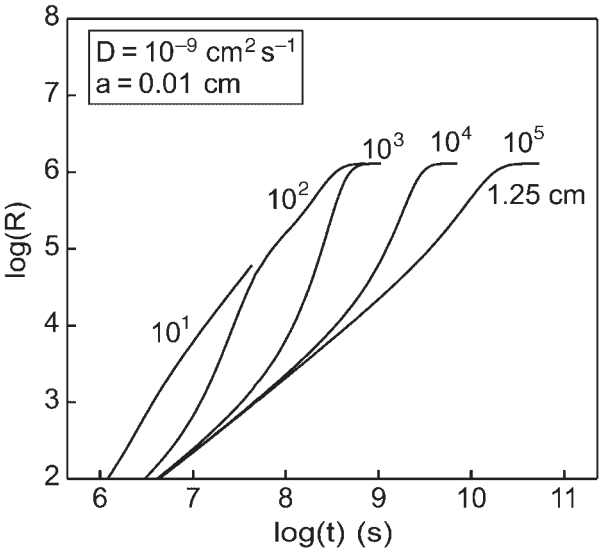

Fig. 2. Log R factor vs log time for various K_D, static case. Each curve shows results for the indicated value of K_D for droplets with the indicated radius a within a spherical shell of melt 1·25 cm in radius. (See text for explanation.)

In Fig. 2 the variation of apparent R factor with time is shown for a series of implicit finite difference simulations for the static spherical drop with the same D but different indicated values of K_D. The time at which the curve begins to steepen is delayed by the effect of a larger K_D, and hastened by smaller K_D, as suggested by Barnes (1993). This effect cannot induce any dispersion of apparent R factor amongst elements that share equal values of K_D.

The model results shown in Figs 1 and 2 are all for situations in which the spherical droplet sits motionless in a static body of silicate melt. In Fig. 3 the effects of droplet settling through static silicate melt are explored using successive applications of equation (7), each using the value of C_{sul} generated by the previous time step. Each curve in Fig. 3 represents the variation of apparent R with time for a single element in sulfide drops of the indicated radius, which are sinking through static silicate melt with a viscosity of 100 Pa s, a typical value for a basaltic liquid (e.g. Ryan & Blevins, 1987). Despite the greater fall velocities associated with increasing droplet radius, the overall effect of increasing the radius is to diminish sharply the flux of metal into the droplet. This occurs because the dependence of R on Dt/a^2 in the first term dominates over $\sqrt{(vt/a)}$ in the second term of equation (7).

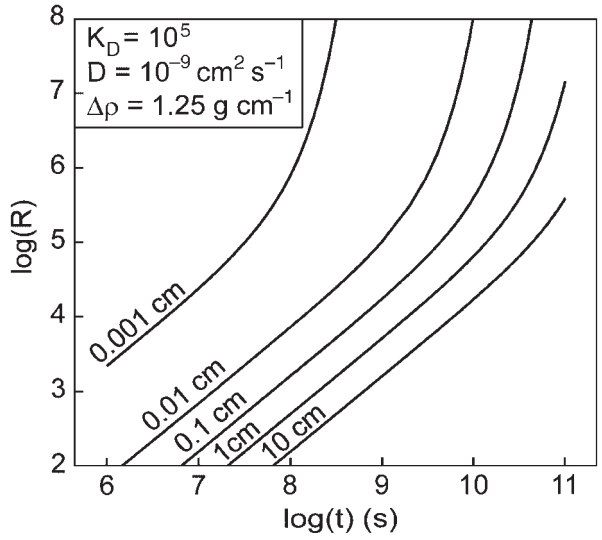

Fig. 3. Log R factor vs log time for sulfide drop falling by Stokes' flow. Each curve shows results for indicated drop radius. (See text for explanation.)

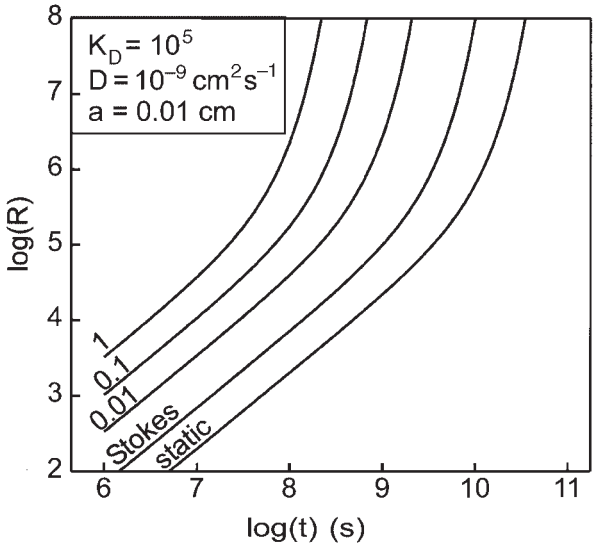

Fig. 4. Log R factor vs log time for sulfide drops in external flows. Each curve shows results for the indicated strain rate (s^{-1}). The curve labelled 'Stokes' is from Fig. 3 for the droplet of the same radius; the curve labelled 'static' is from Fig. 1 for the open system. (See text for explanation.)

In Fig. 4 the effective R factor is shown for a 0·01 cm droplet suspended in a variety of external flows with velocity gradients from an upper limit of $v/L = 1$ s^{-1} (e.g. 10 m s^{-1} change in v over a distance of 10 m) down to zero. These curves were calculated using the numerical application of equation (8). The time dependence of R for Stokes' flow of a 0·01 cm sulfide droplet also appears in Fig. 4 for comparison. The velocity gradient in this case is $\sim 2{\cdot}45 \times 10^{-4}$ s^{-1}, four orders of magnitude less than that expected in a magma flowing rapidly through a dike or lava tube. Also shown for comparison is the curve for the static droplet, reproduced from Fig. 1. Settling of sulfide droplets from a static silicate melt allows only slightly more efficient mass transfer than is expected for static droplets, whereas the introduction of a vigorous externally driven flow can cause important increases in the rate of mass transfer.

In Fig. 5 the rates of metal uptake by sulfide melt pools from static and convected silicate melts are compared. It should be noted that the scales in Fig. 5 are offset by two units in log(R) and four units in log(t) from the preceding diagrams, and that the diffusivity for the metal is at the upper limit of the plausible range (compare with diffusivities in Table 2). The five curves in the upper part of the diagram represent the increase in apparent R with time for sulfide pools being overridden by silicate melts with the indicated velocities, calculated using equation (6). The straight line in the lower part of the diagram shows the dependence of R on time for the sulfide pool under a static body of silicate melt, calculated directly from equation (5). Pools of sulfide melt of economically interesting dimensions under static bodies of silicate melt will not be expected to reach high R over times of the order of 30 Ma.

Even allowing for rapid advection of silicate magma above sulfide pools cannot account for the common observation of high R factor sulfides found at present in massive sulfide bodies. High metal tenors must have been generated in an earlier stage in the evolution of the sulfide in which it was dispersed as small droplets within a silicate magma (see Lesher & Campbell, 1993). This may have occurred before the pools ever formed, as the sulfide was first generated by the liquation event, or it may have occurred during successive disturbances that dispersed the pools into the silicate magma after which it was once more collected into depressions or regions of lower flow velocity. For example, a komatiite channel 100 m wide and 20 m deep, flowing at an average rate of 10 m s^{-1} (upper curve in Fig. 5) for 10^{10} s would would generate a flow with a volume of 2×10^8 km^3 while a subjacent sulfide pool attained an R factor of only 600. This volume is at least an order of magnitude larger than that of the entire Siberian flood basalt province. It seems more probable that observed R factors in Kambalda-type ores can only have been generated by metal transfer into suspended sulfide drops at some time before their eventual collection in pools at the bases of flows. Similarly, massive mineralization in gabbroic systems, exemplified by the Ovoid orebody at Voisey's Bay and the Offset and Sublayer deposits at Sudbury, must result from

Table 2: Estimated diffusivities

			Kambalda[1]	Bushveld[2]	ferrobasalt[3]	Sudbury[4]
		log(η) (Pa s):	−1·37	0·37	2·02	2·39
		Al/alk:	5·49	2·68	1·49	2·42
		T (°C):	1638	1411	1100	1180
		M/O:	0·388	0·25	0·213	0·185
Element	r (Å)	Charge	D (cm^2 s^{-1})	D (cm^2 s^{-1})	D (cm^2 s^{-1})	D (cm^2 s^{-1})
Cu	0·91	1	$9{\cdot}6 \times 10^{-6}$	$1{\cdot}0 \times 10^{-5}$	$5{\cdot}4 \times 10^{-6}$	$2{\cdot}9 \times 10^{-6}$
Au	1·51	1	$1{\cdot}5 \times 10^{-5}$	$3{\cdot}0 \times 10^{-6}$	$5{\cdot}2 \times 10^{-7}$	$2{\cdot}7 \times 10^{-7}$
Ni	0·83	2	$3{\cdot}7 \times 10^{-6}$	$8{\cdot}5 \times 10^{-7}$	$1{\cdot}1 \times 10^{-7}$	$5{\cdot}8 \times 10^{-8}$
Pt	0·94	2	$3{\cdot}2 \times 10^{-6}$	$9{\cdot}2 \times 10^{-7}$	$1{\cdot}4 \times 10^{-7}$	$7{\cdot}3 \times 10^{-8}$
Rh	0·93	2	$3{\cdot}3 \times 10^{-6}$	$9{\cdot}1 \times 10^{-7}$	$1{\cdot}3 \times 10^{-7}$	$7{\cdot}1 \times 10^{-8}$
Pd	1·00	2	$3{\cdot}1 \times 10^{-6}$	$9{\cdot}5 \times 10^{-7}$	$1{\cdot}5 \times 10^{-7}$	$8{\cdot}1 \times 10^{-8}$
Fe	0·92	2	$3{\cdot}3 \times 10^{-6}$	$9{\cdot}0 \times 10^{-7}$	$1{\cdot}3 \times 10^{-7}$	$7{\cdot}0 \times 10^{-8}$
Ir	0·94	2	$3{\cdot}2 \times 10^{-6}$	$9{\cdot}2 \times 10^{-7}$	$1{\cdot}4 \times 10^{-7}$	$7{\cdot}3 \times 10^{-8}$
Os	0·82	3	$6{\cdot}9 \times 10^{-6}$	$2{\cdot}8 \times 10^{-7}$	$6{\cdot}4 \times 10^{-9}$	$3{\cdot}5 \times 10^{-9}$
Ru	0·82	3	$6{\cdot}9 \times 10^{-6}$	$2{\cdot}8 \times 10^{-7}$	$6{\cdot}4 \times 10^{-9}$	$3{\cdot}5 \times 10^{-9}$
Maximum variation in D			5	40	850	830

Sources for melt compositions: [1]komatiite (Williams *et al.*, 1999); [2]marginal intrusion (Harmer & Sharpe, 1985); [3]synthetic ferrobasalt based upon Skaergaard ferrobasalt (Toplis & Carroll, 1995); [4]quartz diorite, Copper Cliff offset dyke (C. Capes & J. E. Mungall, unpublished data, 2001). Viscosity was estimated by the method of Shaw (1972). More information on the parameters Al/alk and M/O and the method of estimation of diffusivities has been given by Mungall (2002*a*).

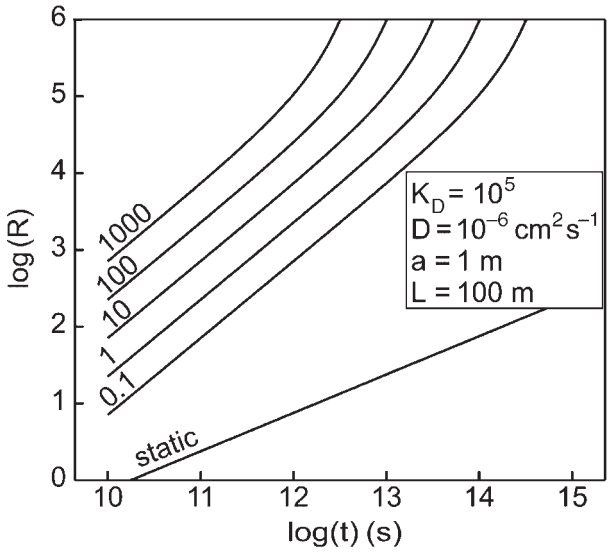

Fig. 5. Log R factor vs log time for sulfide pools adjacent to flowing magma. Each curve shows results for the indicated magma flow velocity. The curve labelled 'static' is the solution for the case of static silicate melt. (See text for explanation.)

collection of sulfide droplets that had already attained a high R factor.

Growth of sulfide droplets

Sulfide droplets grow from infinitesimally small sizes during liquation events, and the relation between droplet size and apparent R factor shown in Fig. 2 might suggest that during the initial stage of droplet growth the very small size of the droplet would lead to essentially instantaneous attainment of extremely high R factors, making the entire discussion irrelevant. The growth of the droplet from an arbitrarily small size within a static silicate melt is accomplished by chemical diffusion of FeS into the droplet. As will be discussed at more length below, both Fe^{2+} and S^{2-} have diffusivities near the middle of the range of diffusivities expected to be observed for chalcophile metals in silicate melts.

Some metals will diffuse into the droplet faster than do Fe^{2+} and S^{2-}, causing the concentrations of those metals to rise in the sulfide droplet faster than they can be diluted by the increased mass of the droplet itself. Other metals will diffuse more slowly than the Fe^{2+} and S^{2-}, so that the droplet grows in volume relatively quickly compared with the rate of addition of the slowly diffusing trace chalcophile metal. The result will be that a slowly diffusing trace metal will not be able to attain a high R factor as long as the sulfide droplet continues to grow.

The concentration of solute in the material being added to the droplet at a given time is the ratio of the flux of

the metal to that of FeS, both being obtained from equation (A21);

$$C_{sul} = \frac{(C_o - C_s)}{C_o^{FeS}} \left(\frac{\frac{D_i}{a} + \sqrt{\frac{D_i v}{4a}}}{\frac{D_{FeS}}{a} + \sqrt{\frac{D_{FeS} v}{4a}}} \right) \quad (12)$$

where D_{FeS} is the diffusivity of the melt component FeS that is feeding the growing droplet C_o^{FeS}, and is the difference between the far-field concentration of FeS and the equilibrium concentration of FeS in the silicate melt at the interface (i.e. the degree of supersaturation of sulfide). Equation (12) cannot be solved directly for rapidly diffusing metals because C_s depends on C_{sul}; unless C_s can be neglected (as for slowly diffusing metals) it cannot be calculated. It can be determined through consideration of the R factor as follows. The mass of an infinitesimal volume dV of the sulfide melt representing new growth from the silicate melt is ρ_{sul}dV; the mass of silicate melt dm estimated through equation (9) can be used with the definition of R to give the following expression for the apparent R factor of the material continuously being added to a growing droplet:

$$R = \frac{1}{C_o^{FeS}} \left(\frac{D_i + 1/2 \sqrt{aD_i v}}{D_{FeS} + 1/2 \sqrt{aD_{FeS} v}} \right). \quad (13)$$

If the droplet is essentially static (i.e. $D_i \gg av$) then equation (13) simplifies to

$$R = \frac{D}{C_o^{FeS} D_{FeS}} \quad (14)$$

whereas if $D_i \ll \sqrt{D_i av}$ (the flow is rapid) then

$$R = \frac{\sqrt{D_i}}{C_o^{FeS} \sqrt{D_{FeS}}}. \quad (15)$$

The values of both C_{sul} and C_s can be determined for both fast- and slow-diffusing metals by calculating R from equation (13), (14) or (15) and applying equations (1) and (2). In the early stages of droplet growth, before settling velocity becomes significant, the value of C_{sul} approaches the equilibrium value set by equation (1) for all cases when

$$D \gg C_o^{FeS} D_{FeS}. \quad (16)$$

Equation (16) indicates that at low degrees of sulfide supersaturation, R factors will be high for all elements, even those that diffuse much more slowly than FeS. If the degree of superaturation is increased, the slowest-diffusing species will show progressively smaller R factors whereas fast-diffusing species remain at high R.

Whatever the initial composition of a growing sulfide droplet, it will converge over time to the composition given by equation (13), (14) or (15), because the original metal budget will be overwhelmed by the composition of the added material as the droplet grows. If a droplet is growing from infinitesimal size during a liquation event then equation (14) will apply initially, but as the droplet increases in size at some time its composition will reflect the onset of Stokes' flow and the reduction in dispersion of apparent R consistent with equation (15).

If the silicate melt is finite, and there are multiple sulfide droplets competing for metals, then at some time the concentration profiles surrounding each droplet will begin to interact, as was considered in the implicit finite difference model used for Figs 1 and 2. There are some interesting and counterintuitive consequences of the transition from disequilibrium to closed system behavior. The true final R factor for the bulk system is equal to the inverse of the initial degree of sulfide supersaturation C_o^{FeS}. Before the concentration profiles of the fastest-diffusing elements within the silicate melt have begun to overlap and interfere with each other, the effective R values for these elements will actually exceed the true bulk R, by a factor equal to D/D_{FeS}. During the time when the diffusion profiles of the fastest-diffusing metals are interacting and drawing down the supply of the fast-diffusing metals but the FeS diffusion profiles are still effectively infinite (i.e. are not interacting) the droplet size will be increasing whereas the total amount of the fast-diffusing element within the droplet will not. In this case, the effective R value shown by the fast-diffusing metal will drop from its high steady-state level attained in the early stage of growth toward a true bulk R value that is set by the ratio of silicate melt mass to the mass of sulfide that will eventually reside in the immiscible droplets. Once the droplet has stopped growing, the slower-diffusing metals will depart from their low steady-state values of apparent R and rise toward concentrations reflecting the true bulk R value of the system.

If sulfide droplets settle out of the silicate melt as they continue to grow, so that they are removed from communication with the silicate melt, they will record apparent R factors for each metal as given by equation (14). In this way, rapidly diffusing chalcophile elements can become significantly fractionated from slowly diffusing elements during the process of formation of a sulfide-rich unit within a larger igneous intrusion. Subsequent deposition of sulfides from the same body of silicate melt, as it continues to exsolve sulfide, will result in the formation of a zoned sulfide deposit, in which the various metals will show peak abundances at different stratigraphic levels depending upon both K_D and D_i.

This effect can be explored by a finite difference model in which a sulfide droplet grows from a small size by the addition of FeS and metals through application of

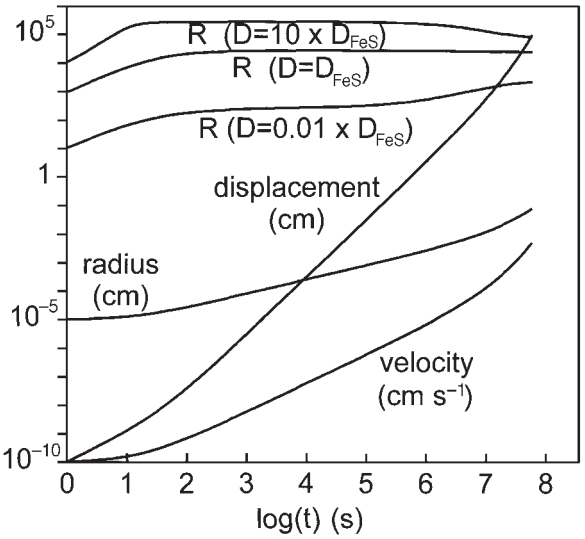

Fig. 6. Growth and settling of sulfide drops. Curves showing the radius, displacement and velocity of a growing drop as it settles by Stokes' flow through a static silicate melt are indicated. Scale units are indicated in parentheses for each curve. The three curves labelled *R* show the effective *R* value for metals whose diffusivities exceed, match or are less than that of FeS, as indicated. (See text for explanation.)

equation (8). At each time step the amount of FeS and metal added by diffusion is calculated. As input to the following time step a new droplet size is determined by addition of the amount of FeS added to the original droplet volume. The velocity in equation (8) is estimated using Stokes' Law for an inviscid droplet [equation (A20)] and used in the following time step. The results are shown in Fig. 6, which shows that the effective *R* values in the droplet after it has settled through 1 km of magma do not differ much from the peak values attained by the droplet in its earlier stage of slow growth and negligible settling velocity. Elements diffusing faster than FeS show slightly decreasing *R* values as the droplet accelerates and falls to the floor, whereas the slower-moving elements benefit from a slight increase in *R* as the droplet moves faster and more undepleted melt is advected close to the sulfide–silicate interface.

Nucleation density

The distance between the nucleation sites of sulfide droplets will play a critical role in the composition and size of the droplets that eventually come to rest at the base of a cooling magma. If droplet nucleation sites are closely spaced (high nucleation density) then the diffusion region surrounding each droplet will soon impinge on those of its neighbors and it will consume all of the excess sulphur and chalcophile metals in its neighborhood, reaching equilibrium quickly. The result will be a magma containing many small, fully equilibrated sulfide droplets whose apparent *R* values correspond to the true mass ratio of silicate to sulfide melt. Collection of these drops would be problematic because their Stokes' flow rates would be negligible, and such finely dispersed sulfide liquid might be transported for great distances in silicate melts without settling to form economically interesting concentrations. Crystal accumulation or flow through constricted spaces between accumulated silicate phases (e.g. phenocrysts or xenoliths) would promote their collection and deposition, perhaps accounting in part for the common association between abundant xenoliths and sulfide concentrations (e.g. Voisey's Bay, Noril'sk, Sudbury).

If the nucleation sites are widely spaced, then the droplets will continue to grow for a long time before their diffusion regions begin to interact with those surrounding other droplets. At extremely low nucleation density, the growing droplets will remain effectively isolated from all other droplets until they have grown so large that they rapidly settle out of the melt by Stokes' flow. In this latter case, the result will be the deposition at the base of the magma body of a few relatively large sulfide droplets whose compositions are controlled kinetically through equation (13).

Because of the energy barrier to nucleation of new sulfide droplets within silicate melt, the primary controls on nucleation density are the surface energy of the sulfide–silicate melt interface and the degree of supersaturation (Dowty, 1980). Low degrees of supersaturation and high surface tension will conspire to inhibit nucleation. Sulfide–silicate melt interfaces show surface tension between two and 10 times those typical of silicate melt–silicate solid interfaces (Dowty, 1980; Ip & Toguri, 1993), possibly promoting substantial delays in nucleation of sulfide droplets within the silicate melt. Heterogeneous nucleation of sulfide droplets on silicate minerals would also be inhibited because interfacial energies between sulfide melt and silicate solids are similarly high (Ip & Toguri, 1993). The solubility of sulfide in magmas is an increasing function of temperature (e.g. Wendlandt, 1982). Thus if a magma is cooled through the sulfide saturation temperature it is to be expected that nucleation of sulfide droplets will lag substantially behind that of silicate phases, that the nucleation sites will be widely spaced, and that the resulting small number of sulfide droplets will continue to grow in effective isolation from one another until they have attained sufficient size to settle to the bottom. Because low nucleation densities result from small degrees of supersaturation of the major solute species (FeS in this case), the term $1/C_o^{FeS}$ will tend to be large, leading to large apparent *R* values.

If a magma is abruptly perturbed into a state of substantial sulfide supersaturation, then the number of nucleation sites will be much larger, and fully equilibrated compositions are to be expected in the resultant sulfide

deposits. Thus sulfide ores generated by magma mixing events are likely to show compositions that can be described by equations (1) and (2), whereas the conditions for kinetically controlled PGE abundances in sulfides and consequent stratigraphic offsets between peak abundances of different metals are more likely to be met whenever a magma reaches sulfide saturation by passively cooling through the sulfide saturation temperature.

Naturally occurring sulfide droplets trapped in glassy basaltic rocks are likely to suffer from the effects described here, as they must have undergone extreme departures from equilibrium during the short time leading up to their entrapment as globules in a glass matrix. It would be interesting to look for evidence of such effects, particularly as currently accepted estimates of sulfide–silicate partition coefficients for the PGE and Au are largely based on measured concentrations in these natural occurrences (e.g. Peach *et al.*, 1990).

Experimental determinations of partition coefficients might be subject to dispersion of apparent R and hence K_D as a result of differences in D between elements. There are two factors that mitigate against such erroneous results being misinterpreted as equilibrium K_D. First, a well-executed experimental study will include a demonstration of the likelihood of an approach to equilibrium, generally through reversals of starting conditions or time series. In either case, the kinetic effects described here would be apparent as evidence for a failure to reach equilibrium, and the results would be discarded. Second, high-temperature experimental charges typically are <1 cm in size, and distances between sulfide droplets are of the order of 0·1 mm. Qualitative extrapolation of the results in Fig. 1 indicates that equilibrium should be reached after a maximum of 10^5 s (about 1 day) for droplet spacings and radii <0·1 mm. Experimenters constrained to shorter run durations or the use of single large sulfide melt volumes in large capsules should consider the possibility of kinetic effects on measured K_D.

APPLICATION TO NATURAL SYSTEMS

Choice of model parameters

The analytical and numerical models presented in the previous section require estimates of several parameters to be applied to natural systems. The geometry and flow characteristics may vary widely, and the appropriate choices should generally be self-evident. There are several schemes available in the literature for estimating melt viscosities (e.g. Bottinga & Weill, 1972; Shaw, 1972). Melt densities can similarly be estimated (e.g. Kress & Carmichael, 1991; Kucharski *et al.*, 1994) and do not influence the outcome of the models very strongly in any case.

The diffusivities of the chalcophile trace elements are the most difficult parameters to estimate. Experimental data for diffusivities of the chalcophile elements are almost entirely lacking; however, a recent parameterization of published diffusivities of other cations in silicate melts can be used to estimate D if the oxidation states and cation radii are known (Shannon, 1976; Mungall, 2002*a*). It is beyond the scope of this paper to review the often contradictory literature regarding redox states of chalcophile trace elements, and I have selected the following most probable oxidation states for the PGE and other chalcophile metals in basaltic silicate magmas, assuming that they are present as monatomic cations rather than as clusters or more complex molecular species in the melt: Os^{3+} (Borisov & Walker, 1998), Ir^{2+} (Borisov & Palme, 1995; O'Neill *et al.*, 1995), Rh^{2+} (Ertel *et al.*, 1999), Ru^{3+} (Borisov & Nachtweyh, 1998), Pt^{2+} (Borisov & Palme, 1997; Ertel *et al.*, 1999), Pd^{+} and Pd^{2+} (Borisov *et al.* 1994), Au^{+} (Borisov & Palme, 1996), Cu^{+} (Ripley & Brophy, 1995; Holzheid & Lodders, 2001), Ni^{2+} (Ertel *et al.*, 1997), Fe^{2+}. Both Os^{3+} and Ru^{3+} are high field strength elements (HFSE; field strength >10). Field strength here is defined as the square of the nominal charge divided by Shannon's (1976) ionic radius for octahedral coordination. Where cation radii are not listed by Shannon they were estimated by extrapolation or interpolation on plots of radius vs oxidation state. Estimated diffusivities for these cations in a variety of melts appear in Table 2. HFSE diffusivities tend to be subequal in all melts, so that any highly charged chalcophile metal ion can be assumed to show diffusivity that can be estimated using the Eyring equation (e.g. LaTourette *et al.*, 1996; Mungall *et al.*, 1999; Mungall, 2002*a*). Low field strength elements (LFSE: field strength <1) show a wide range in diffusivity, controlled strongly by the radius of the diffusing cations. The diffusivity of Cu^{+} estimated using the method of Mungall (2002*a*) is generally the largest among the elements of interest; that of Au^{+} is somewhat less. Intermediate field strength elements (IFSE) can show large differences in diffusivity, ranging over as much as three orders of magnitude in relatively siliceous melts, but less than one order of magnitude in basaltic liquids (see Lowry *et al.*, 1982; Henderson *et al.*, 1985; LaTourette *et al.*, 1996; Mungall *et al.*, 1999; Mungall, 2002*a*). The group of IFSE of possible interest (e.g. Pt^{2+}, Pd^{2+}, Rh^{2+}, Ir^{2+}, Ni^{2+}, Fe^{2+}) have similar radii and are likely to show diffusivities intermediate between the extremes of the IFSE and HFSE.

The melt components most important to the growth of sulfide droplets are Fe^{2+} and S^{2-}. The diffusivity of sulphur in silicate melts is poorly known and cannot be estimated using Mungall's (2002*a*) empirical approach. Comparison of data presented by Watson (1994) and by Lowry *et al.* (1982) indicates that the diffusivities of these ions are probably subequal in basaltic and andesitic melts,

ranging from about 10 times that of the slowest moving HFSE at ~1100°C to subequal to the HFSE diffusivities at high temperatures (~1600°C). An approximate FeS diffusivity is estimated for each melt in Table 2, based on the assumption that Fe^{2+} and S^{2-} have similar diffusivities, which can be predicted based on the relatively well-constrained diffusivity of Fe^{2+}.

To aid in comparison of the diffusivities shown in Table 2, the bottom row contains the approximate ratio between the fastest- and slowest-diffusing cations in each melt. Recalling that for most of the possible sulfide–silicate melt geometries considered here, there is a direct linear relation between effective R value and diffusivity, it is obvious that the potential for dispersion of effective R values is great at Sudbury and progressively less important at the Bushveld Complex, in ferrobasalts, or at Kambalda. In any scenario involving open system behavior at Sudbury, samples of sulfide that preserve the compositions of original droplets of sulfide liquid should be expected to display dispersions in R value amongst different metals in the same sulfide droplet of as much as three to four orders of magnitude. In contrast, by using the spread in diffusivities suggested in Table 2 in equation (8) one would expect to see that the R values recorded by massive sulfide pools at Kambalda should show dispersions of $\sim\sqrt{10}$, i.e. a factor of about three. Relative variations of R by a factor of three may be undetectable, given the large scatter typically observed in trace element abundances in sulfide ores and the persistent uncertainty in K_D (e.g. Fleet *et al.*, 1999).

Comparison with ore compositions

Kambalda

Kambalda, Australia, is the type locality for komatiite-hosted magmatic Ni–Cu sulfide deposits, which are typically thin (<10 m) massive sulfide lenses overlain by thicker (tens to hundreds of meters) disseminated sulfide zones hosted by large peridotite bodies inferred to represent a channel-filling facies of lava rivers (e.g. Lesher & Campbell, 1993). The role of kinetics in controlling R values of metals contained in Kambalda-type deposits must be rather slight as a result of the relatively small dispersion in probable diffusivities indicated in Table 2. Lesher & Campbell (1993) modeled the evolution of komatiite-hosted massive and disseminated sulfide mineralization at Kambalda with a flexible approach allowing for the use of variable effective partitioning coefficients for each metal. In such an approach, kinetic effects on effective partitioning behavior should readily become apparent, but Lesher & Campbell (1993) found it necessary to propose variations in the K_D only of Ni. As the partitioning behavior of Ni is known to depend rather strongly upon f_{O_2} and f_{S_2}, parameters that may have varied widely during ore formation at Kambalda, there is no need to appeal to kinetic effects as controls on partitioning behavior. Comparison of disseminated and massive ore compositions at Alexo (Barnes & Naldrett, 1986) also shows no systematic variation in metal ratios that could be attributed to kinetic controls on metal partitioning.

As discussed above, it is probable that sulfides at present contained in massive sulfide ore-bodies at Kambalda underwent at least one phase of their evolution as finely dispersed suspensions of sulfide droplets in the komatiite magma before they finally settled into pools. The rate of mass transfer from komatiite into pools would be too slow to permit the attainment of the observed R values in times less than several hundred years.

Bushveld Complex

The stratiform PGE–Ni–sulfide deposits of the Bushveld complex have been the subject of numerous studies (e.g. von Gruenewaldt *et al.*, 1985; Maier & Barnes, 1999; Ballhaus & Sylvester, 2000). Although there remains some controversy over the extent to which hydrothermal processes have modified or even generated the deposits (e.g. Boudreau *et al.*, 1986; Boudreau & Meurer, 1999), the evidence is compelling that the sulfides were derived from the overlying silicate melt in a liquation event, and collected at approximately their present location as part of a cumulate sequence related to a magma-mixing event. Considering the 100-fold variation in expected values of D for various metals in the Bushveld U-type magma thought to have been present in the magma chamber at the time, there seems to be ample opportunity to observe kinetic effects on trace chalcophile element behavior.

Maier & Barnes (1999) and Barnes & Maier (2002) have compiled existing data for chalcophile element abundances in stratiform deposits of the Bushveld Complex and compared them with the compositions of unmineralized horizons and with the probable composition of the parent silicate magmas [B1 magma of Davies & Tredoux (1985)]. A comprehensive review of the compositions of the stratiform deposits of the Bushveld Complex is clearly beyond the scope of this paper, but some qualitative points can be made.

To a first approximation, all of the PGE are present at abundances consistent with derivation from the parent silicate magmas at R values of the order of 10^4–10^5 in the Merensky, Bastard, Pseudo and Tarentaal reefs using experimentally determined K_D for PGE (Fleet *et al.*, 1996; Ballhaus & Sylvester, 2000). Furthermore, there is no apparent cryptic layering in the PGE abundances within or around the Merensky reef; that is, the composition of the sulfide fraction of the rock seems invariant through the immediate section of stratigraphy including the Merensky reef (Barnes & Maier, 2002).

Maier & Barnes (1999) have observed that several of the lower stratiform deposits show moderate increases in the proportions of IPGE (Os, Ir, Ru) over PPGE (Rh, Pt, Pd) above those that could be consistent with extraction of sulfide melt from silicate magma when all six elements are thought to have similar values of K_D. They suggested that relative variations in the abundances of IPGE and PPGE could be related to the effects of crystallization of monosulfide solid solution (mss) from sulfide melts after formation of the stratiform deposits. In this scenario, IPGE-rich mss-bearing sulfide material has remained behind after preferential removal of residual PPGE-rich sulfide melt into an upward-percolating intratelluric silicate melt.

If the kinetic processes described in this paper were responsible for the observed moderate increases in PPGE abundances over IPGE abundances, the two elements with the smallest diffusivities (Os, Ru) would be expected to be significantly fractionated from the remaining IPGE Ir, because of Ir's larger expected diffusivities; furthermore, the tendency would be for ores to be impoverished rather than enriched in Os and Ru, whereas Barnes & Maier (2002) have shown that the Os and Ru abundances appear to reflect the presence of excess IPGE-rich (i.e. Os-rich) monosulfide solid solution cumulate material. As the inter-element variations are contrary to the results anticipated from kinetic fractionation and there is no evidence for inter-element offsets in the PGE profiles in the reefs, it appears unlikely that kinetics have played any significant role in controlling ore compositions in the Bushveld Complex. The reefs appear to have formed from fully equilibrated sulfide droplets in a manner consistent with their apparent origin through turbulent magma mixing events.

Sudbury

The Sudbury igneous complex is thought to be a melt sheet produced by a large bolide impact at ~1849 Ma (e.g. Dietz, 1964; Grieve, 1994). Liquation of sulfide melt accompanied or preceded the first appearance of silicate minerals in the originally superheated melt sheet, generating a series of important Ni–Cu–PGE deposits at the base of the magma body (Hawley & Stanton, 1962; Naldrett *et al.*, 1982, 1999). The large range in estimated diffusion coefficients for the primary Sudbury magma as shown in Table 2 implies that chalcophile metals should have been especially prone to kinetic fractionation at Sudbury. At Sudbury there is commonly a halo of disseminated sulfide up to several hundred meters wide above the massive ores at the base (e.g. Naldrett *et al.*, 1999), which would be expected to show extreme kinetic fractionation if they had formed by a process involving fractional segregation. Such effects are not shown at Sudbury, and the compositions of sulfides there are thought to result from equilibrium partitioning at relatively low R near 1000, followed by protracted fractional crystallization of monosulfide solid solution (Naldrett *et al.*, 1999). Mungall (2002*b*) has shown that the disseminated sulfide haloes at Sudbury probably result from the percolation of fractionated sulfide liquid back up into the silicate cumulates at a late stage in the evolution of the system, rather than from any process involving fractional segregation at low degrees of sulfide supersaturation.

Munni Munni

The Munni Munni intrusion is an Archean layered intrusion in Australia comprising a cyclically layered Ultramafic Series (UMS) capped by a Gabbroic Series (GS) (Donaldson, 1974; Hoatson & Keays, 1989; Barnes *et al.*, 1990; Barnes, 1993). The transition from the UMS to the GS is thought to reflect a transition from a periodically replenished magma chamber occupied by Mg-rich magma to closed system crystallization from a more evolved Fe-rich tholeiitic magma (Barnes *et al.*, 1990). The uppermost cyclic unit of the UMS is a websterite layer ~30 m thick containing disseminated Cu-rich sulfides with high and variable PGE tenors. The sulfide horizon occurs as a single stratigraphic unit throughout the exposed portion of the intrusion, and is interpreted to represent the onset of fractional segregation of sulfide from the silicate magma (Hoatson & Keays, 1989; Barnes *et al.*, 1990; Barnes, 1993). Chalcophile metal concentrations and tenors show systematic variations with stratigraphic height through the sulfide layer (Fig. 7). Within a given section, there is typically a lower PGE-enriched layer in which all chalcophile elements are enriched at the same stratigraphic level (coincident layer), and another, stratigraphically higher layer in which each PGE shows a distinct peak in concentration at a particular stratigraphic level, but the elevation of each element's peak is offset from those of other elements (offset layer). The offset pattern is repeated in the same sequence in all instances where it can be observed, with Pd abundance peaking at the lowest level, followed by other PGE, then Au, and finally Cu and Ni.

The offset sulfide horizon in the Munni Munni intrusion is interesting because it is a particularly well-documented representative of similar features of several other layered intrusions. The Great Dyke of Zimbabwe (Naldrett & Wilson, 1990; Wilson & Tredoux, 1990), the Skaergaard Intrusion of Greenland (Andersen *et al.*, 1998), and the Rinçon del Tigre Intrusion of Brazil (Prendergast, 2000) each show similar offset PGE-rich sulfide-bearing layers, which are major exploration targets. Strong arguments supporting the interpretation that the offset layers at Munni Munni preserve primary igneous layering in modal abundance of sulfide were given by Barnes (1993). The availability of published PGE, Au, Cu and

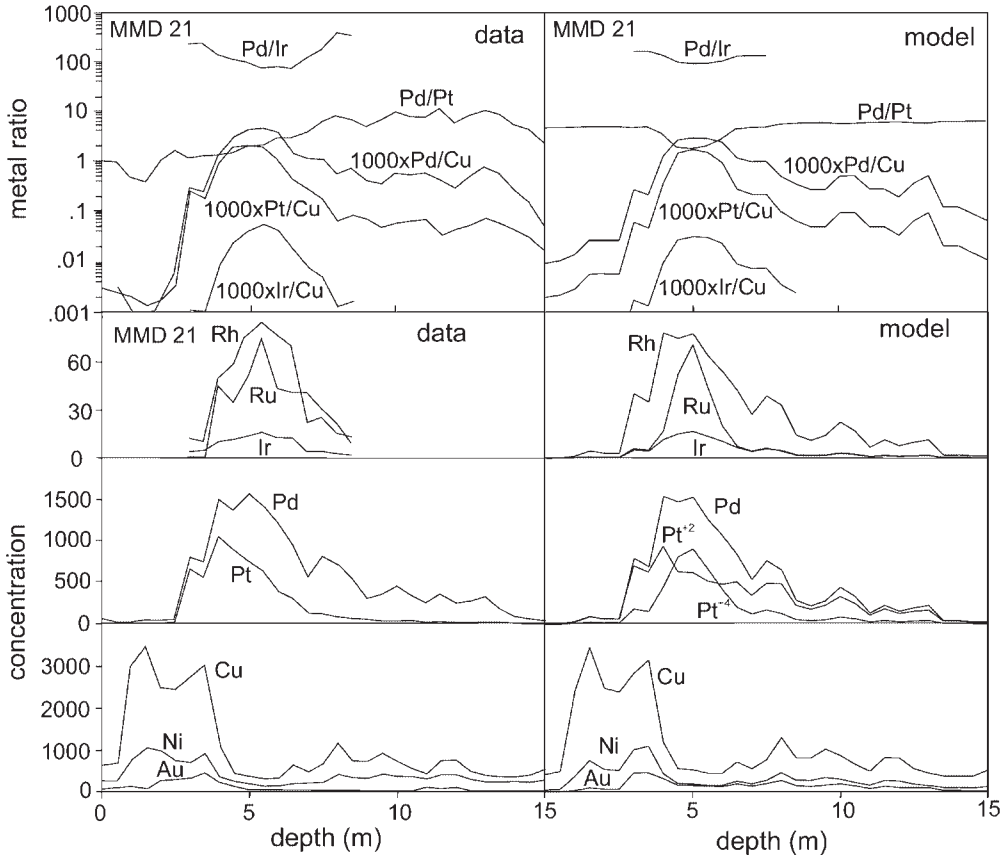

Fig. 7. Chalcophile element distribution vs depth below the top of the sulfide zone at Munni Munni. Data are from Barnes (1993); model results are described in the text. The two model curves for Pt show results for indicated oxidation states; the model ratios involving Pt were calculated assuming that Pt was quadrivalent. (See text for discussion.)

Ni contents in continuous samples throughout the sulfide layer at Munni Munni make it especially well suited for detailed analysis and modeling (e.g. Barnes, 1993). Barnes *et al.* (1990) showed that the gross pattern of offset layers could be accounted for by fractional segregation of small amounts of sulfide melt from a magma column several hundred meters high (e.g. Naldrett & Wilson, 1990). However, Barnes (1993) showed that in detail there are several features of the offset profiles that cannot be reconciled with the fractional segregation model if instantaneous equilibrium is assumed between sulfide and silicate melt, through the imposition of constant equilibrium K_D values. Rather, Barnes (1993) found that the profiles could be modeled only by proposing that partitioning coefficients varied through orders of magnitude during the time taken to deposit the several meters of cumulates containing the offset sulfide layer. Barnes' modeling of the profiles relied on *ad hoc* variations in K_D to reproduce the data. He suggested that variations in intensive parameters such as f_{O_2} might affect the partitioning coefficients but concluded that there was no petrological evidence for such excursions. Barnes instead favored a hypothesis involving the prior existence of platinum group minerals suspended in the host silicate magma and their collection by newly formed sulfide melt. In the following section, I show how the kinetic model of sulfide fractional segregation accounts well for the peculiarities of the offset profile that cannot be accommodated by equilibrium models of sulfide segregation, providing a mechanism for the variations in effective partitioning behavior originally proposed by Barnes (1993).

I have followed Barnes (1993) and Naldrett & Wilson (1990) in my approach to modeling the evolution of a cumulate layer including sulfides that are forming by fractional segregation from the overlying silicate magma. The calculation is performed on a spreadsheet as a series of discrete sequential sulfide segregation events. At each step a new 0·5 m thickness of websterite is assumed to have formed; its sulfide content is estimated from the Cu content of the actual rock in that interval (see Barnes, 1993). The metals contained in this quantity of sulfide are removed from the overlying melt and the overlying silicate melt composition is recalculated. This approach

is essentially identical to that followed by Barnes (1993) and Naldrett & Wilson (1990), except that whereas they used equations (1) and (2) to establish the composition of the sulfide liquid being removed, I have used equation (14).

Input to equation (14) are estimates of the partition coefficients and diffusion coefficients of all the metals of interest, initial silicate melt composition, and degree of sulfide oversaturation at each step. The initial melt composition was assumed to be 200 ppm Cu, 150 ppm Ni, and 0·1, 0·5, 0·6, 11, 12, and 5 ppb, respectively, for Ir, Ru, Rh, Pt, Pd, and Au. These starting values were chosen to be consistent with the chosen partitioning coefficients and observed sulfide compositions. The estimate of sulfide content of the rock from whole-rock Cu analyses was made by multiplying Cu (ppm) by $5{\cdot}4 \times 10^{-6}$ (e.g. 400 ppm Cu $\times$ $5{\cdot}4 \times 10^{-6} = 0{\cdot}216\%$ sulfide in the rock). [For a more detailed discussion of this approach, see Barnes (1993).] Diffusion coefficients were assumed to be the same as were calculated for the U-type magma of the Bushveld complex (Table 2), which formed an ultramafic layered series similar to that observed at Munni Munni, except that the crystallization sequence at the Bushveld was olivine–orthopyroxene–plagioclase as opposed to olivine–clinopyroxene–plagioclase at Munni Munni. Similar results were obtained using the ferrobasalt parameters in Table 2 (not shown here). All whole-rock data for the sulfide horizon at Munni Munni were obtained by digitizing the figures presented by Barnes (1993). Partition coefficients for chalcophile elements were 25 000 for Pt, 60 000 for other PGE, 18 000 for Au, 1000 for Cu, and 500 for Ni (see Peach *et al.*, 1990; Fleet *et al.*, 1999). The choice of a smaller K_D for Pt was predicated on the common observation that Pd is depleted slightly faster than Pt upsection in layered intrusions (e.g. Maier & Barnes, 1999). The height of the magma column was assumed to be 2000 m, consistent with the suggestion of Barnes *et al.* (1990) that the entire GS crystallized from a closed magma body directly on top of the sulfide horizon.

All metal concentrations were estimated by inverting equation (14) to find the C_o^{FeS}dictated by actual Pd concentration with D, K_D fixed as described above, and then using this value of C_o^{FeS} in equation (14) to set the concentrations of the other elements in the sulfide. The whole-rock metal concentrations were found by multiplying the sulfide concentration by the sulfide fraction, i.e. I have assumed that the silicate portion of the rock was entirely devoid of chalcophile metals. The modeled compositions of the offset sulfide layer were therefore rigidly set by the initial choices of melt composition, D and K_D, and by the assumptions behind the application of equation (14). No further iterative modification of any model parameter was used, so that the results of the modeling are entirely self-consistent and based on a single reasonable set of initial assumptions. It is worth noting also that the results shown below were not the product of a long interative process of selection of model parameters; all parameters used were as initially chosen based on a review of the literature, and none had to be adjusted to make the model fit the data.

Figure 7 is a comparison of measured and modeled element abundance vs stratigraphic height (as depth below the top of the sulfide horizon) for the section labelled MMD21 by Barnes (1993). Two curves are shown for the model concentration of Pt, one calculated assuming that Pt is in the divalent state with an initial concentration in the silicate melt of 11 ppb, the other for quadrivalent Pt with an initial concentration in the silicate melt of 15 ppb. The model using Pt^{4+} provides a better match to the data than does the Pt^{2+} model; however, in both cases the correspondence between model and data is satisfactory to the extent that the positions and general shapes of all of the peaks are reproduced well, as are the shapes of the ratios of Ir/Cu, Pt/Cu, Pd/Cu, and Pd/Ir. The major exception to the goodness of fit for divalent Pt is the presence in the model of a considerable amount of Pt below its main peak, whereas the actual data show a rather steeper rise below the peak. Apart from this discrepancy the match is strikingly good. Comparing the quality of these fits with that achieved by Barnes (1993) with constant K_D and an equililibrium partitioning model, and recalling his conclusion that 'the observed decoupling between PGE and sulfide distribution in the offset layer cannot be adequately modeled by a fractional sulfide segregation model', it is evident that the kinetic model offers a substantial improvement over equilibrium models, while avoiding the adoption of *ad hoc* variations in the parameters governing the model.

Although differences among diffusivities of the PGE do exert some control on the outcome of the model, the first-order control is exerted by the degree of supersaturation. Since the application of equation (2) implicitly assumes the same R factor for each element in the system, variations in behavior between elements in equilibrium models must be accommodated by proposing that their K_D values can vary arbitrarily. The kinetic model permits variations in R factor while keeping K_D constant, although achieving the same effect as if the K_D were being varied. The degree of sulfide supersaturation implied by the model (Fig. 8) initially shows a gradually steepening decrease in sulfide supersaturation, reaching extremely small values at the time when the main Pd peak was formed. Immediately following this is a second stage in which the magma becomes strongly sulfide supersaturated. The means by which such a fluctuation in degree of sulfide supersaturation might be induced is not obvious; however, the object of this exercise has not been to try to establish exactly what the values of the

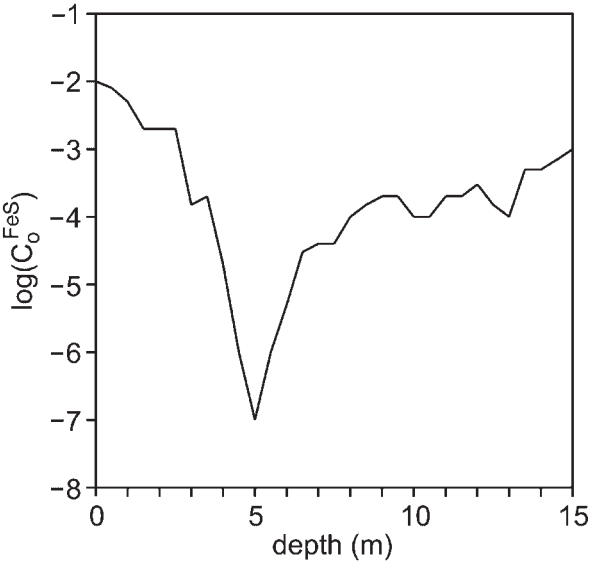

Fig. 8. Degree of modeled FeS supersaturation vs depth below the top of the sulfide zone at Munni Munni. (See text for discussion.)

model parameters might have been. The solution shown in Fig. 7 is non-unique and may be missing some important details such as magma recharge. The main objective of the exercise has been to show that the kinetic model can account for the observed variation of PGE abundance with suitable choice of parameters.

CONCLUSIONS

The principal conclusion of this paper is that wherever sulfide liquation occurs in a silicate magma there is a potential for growth and collection of sulfide droplets whose compositions are largely controlled by kinetic factors rather than equilibrium metal partitioning. The dominant controls on the kinetic fractionation of metals are imposed by the diffusivities of the metals in the silicate melt, by the size of the sulfide body, by the strain rate in the enclosing silicate melt, and by the duration of the event in which the two melts coexist.

The faster-diffusing elements in a given system will tend to show larger apparent R values than will slowly diffusing elements, and the span in apparent R may exceed five orders of magnitude. The most mobile elements are likely to be Cu and Au; intermediate diffusivities are anticipated for Pt, Pd, Ir, Ni, and Rh; the slowest are probably Os and Ru and possibly also Pt. Rapid movement of silicate melt adjacent to bodies of sulfide dramatically speeds the approach to equilibrium. Small droplets reach equilibrium faster than large ones; sulfide pools cannot reach equilibrium even with rapidly moving silicate melt on time scales appropriate for the formation of magmatic ore deposits.

Large surface energies between sulfide and silicate melt may retard the nucleation of sulfide melt sufficiently to permit widely spaced sulfide droplets to nucleate, grow, and settle out of their host silicate magmas without interacting significantly with one another. Droplets grown in this way, from persistently sulfide-supersaturated silicate melts, will preserve compositions controlled by kinetic effects. The fractional segregation of kinetically fractionated sulfide melts in large, quiescent layered intrusions is a plausible mechanism for the generation of offset PGE abundance profiles. Segregation of sulfide showing large apparent R values does not require the equilibration of large volumes of silicate melt with the sulfide droplets, but can result from removal of small amounts of sulfide from any amount of silicate melt at small degrees of sulfide supersaturation. Application of the kinetic model to the offset PGE profiles at the Munni Munni intrusion in Australia succeeds in reproducing observed element distributions whereas models based on equilibrium partitioning cannot.

The kinetic effects predicted here may be encountered in a wide variety of settings, and should be considered as possible controls on sulfide compositions in any magmatic system.

REFERENCES

Andersen, J. C. O., Rasmussen, H., Nielsen, T. F. D. & Rønsbo, J. R. (1998). The triple group and the platinova gold and palladium reefs in the Skaergaard intrusion: stratigraphic and petrographic relations. *Economic Geology* **93**, 488–509.

Ballhaus, C. & Sylvester, P. (2000). Noble metal enrichment processes in the Merensky Reef, Bushveld Complex. *Journal of Petrology* **41**, 545–561.

Barnes, S. J. (1993). Partitioning of the platinum group elements and gold between silicate and sulfide magmas in the Munni Munni Complex, Western Australia. *Geochimica et Cosmochimica Acta* **57**, 1277–1290.

Barnes, S.-J. (1998). Possible causes of high Pd/Pt, Pd/Ir, Rh/Ir, Pd/Os ratios in sulfide ores. *GAC–MAC Program with Abstracts* **1998**, A9.

Barnes, S.-J. & Maier, W. D. (2002). Platinum-group elements and microstructures of normal Merensky Reef from Impala Platinum Mines, Bushveld Complex. *Journal of Petrology* **43**, 103–128.

Barnes, S.-J. & Naldrett, A. J. (1986). Variations in platinum group element concentrations in the Alexo mine komatiite, Abitibi greenstone belt, northern Ontario. *Geological Magazine* **123**, 515–524.

Barnes, S. J., McIntyre, J. R., Nisbet, B. W. & Williams, C. R. (1990). Platinum-group element mineralization in the Munni Munni Complex, Western Australia. *Mineralogy and Petrology* **42**, 141–164.

Boudreau, A. E. & Meurer, W. P. (1999). Chromatographic separation of the platinum-group elements, gold, base metals and sulfur during degassing of a compacting and solidifying igneous crystal pile. *Contributions to Mineralogy and Petrology* **134**, 174–185.

Boudreau, A. E., Mathez, E. A. & McCallum, I. S. (1986). Halogen geochemistry of the Bushveld and Stillwater complexes: evidence for the transport of the platinum-group elements by Cl-rich fluids. *Journal of Petrology* **27**, 967–986.

Borisov, A. & Nachtweyh, K. (1998). Ruthenium solubility in silicate melts: experimental results at oxidizing conditions. In: *Lunar and Planetary Science XXIX*. Houston, TX: Lunar and Planetary Institute, Abstract 1320 (CD-ROM).

Borisov, A. & Palme, H. (1995). The solubility of iridium in silicate melts: new data from experiments with $Ir_{10}Pt_{90}$ alloys. *Geochimica et Cosmochimica Acta* **59**, 481–485.

Borisov, A. & Palme, H. (1996). Experimental determination of the solubility of gold in silicate melts. *Mineralogy and Petrology* **56**, 297–312.

Borisov, A. & Palme, H. (1997). Experimental determination of the solubility of platinum in silicate melts. *Geochimica et Cosmochimica Acta* **61**, 4349–4357.

Borisov, A. & Walker, R. J. (1998). Osmium solubility in silicate melts: new efforts and new results. *Lunar and Planetary Institute Contribution* **957**, 2–3.

Borisov, A., Palme, H. & Spettel, B. (1994). Solubility of palladium in silicate melts: implications for core formation in the Earth. *Geochimica et Cosmochimica Acta* **58**, 705–716.

Bottinga, Y. & Weill, D. F. (1972). The viscosity of magmatic silicate liquids: a model for calculation. *American Journal of Science* **272**, 438–475.

Brügmann, G. E., Naldrett, A. J., Asif, M., Lightfoot, P. C., Gorbachev, N. S. & Fedorenko, V. A. (1993). Siderophile and chalcophile metals as tracers of the evolution of the Siberian Trap in the Noril'sk region, Russia. *Geochimica et Cosmochimica Acta* **57**, 2001–2018.

Campbell, I. H. & Naldrett, A. J. (1979). The influence of silicate:sulfide ratios on the geochemistry of magmatic sulfides. *Economic Geology* **74**, 1503–1506.

Campbell, I. H., Naldrett, A. J. & Barnes, S. J. (1984). A model for the origin of the platinum-rich sulfide horizons of the Bushveld and Stillwater Complexes. *Journal of Petrology* **24**, 133–165.

Crank, J. (1975). *The Mathematics of Diffusion*, 2nd edn. Toronto, Ont.: Oxford University Press, 414 pp.

Davies, G. & Tredoux, M. (1985). The platinum-group element and gold contents of the marginal rocks and sills of the Bushveld Complex. *Economic Geology* **80**, 838–848.

Dietz, R. S. (1964). Sudbury structure as an astrobleme. *Journal of Geology* **72**, 412–434.

Donaldson, M. J. (1974). Petrology of the Munni Munni Complex, Roeburne, Western Australia. *Journal of the Geological Society of Australia* **21**, 1–16.

Dowty, E. (1980). Crystal growth and nucleation theory and the numerical simulation of igneous crystallization. In: Hargraves, R. B. (ed.) *Physics of Magmatic Processes*. Princeton, NJ: Princeton University Press, pp. 419–485.

Ertel, W., Dingwell, D. B. & O'Neill, H. St. C. (1997). Composition dependence of the activity of Ni in silicate melts. *Geochimica et Cosmochimica Acta* **61**, 4704–4721.

Ertel, W., O'Neill, H. St. C., Sylvester, P. J. & Dingwell, D. B. (1999). Solubilities of Pt and Rh in a haplobasaltic silicate melt at 1300°C. *Geochimica et Cosmochimica Acta* **63**, 2439–2449.

Fleet, M. E., Crocket, J. H. & Stone, W. E. (1996). Partitioning of platinum-group elements (Os, Ir, Ru, Pt, Pd) and gold between sulfide liquid and basalt melt. *Geochimica et Cosmochimica Acta* **60**, 2397–2412.

Fleet, M. E., Crocket, J. H., Liu, M. & Stone, W. E. (1999). Laboratory partitioning of platinum-group elements (PGE) and gold with application to magmatic sulfide–PGE deposits. *Lithos* **47**, 127–142.

Gautschi, W. (1972) Error function and Fresnel integrals. In: Abramovitz, M. & Stegun, I. A. (eds) *Handbook of Mathematical Functions with Formulas, Graphs, and Mathematical Tables. National Bureau of Standards Applied Mathematics Series* **55**, 295–329.

Grieve, R. A. F. (1994). An impact model of the Sudbury structure. *Ontario Geological Survey Special Volume* **5**, 119–132.

Harmer, R. E. & Sharpe, M. R. (1985). Field relations and strontium isotope systematics of the marginal rocks of the Eastern Bushveld Complex. *Economic Geology* **80**, 813–837.

Hawley, J. E. & Stanton, R. L. (1962). The facts: the ores, their minerals, metals and distribution. *Canadian Mineralogist* **7**, 30–145.

Henderson, P., Nolan, J., Cunningham, G. C. & Lowry, R. K. (1985). Structural controls and mechanisms of diffusion in natural silicate melts. *Contributions to Mineralogy and Petrology* **89**, 263–272.

Hoatson, D. M. & Keays, R. R. (1989). Formation of platiniferous sulfide horizons by crystal fractionation and magma mixing in the Munni Munni layered intrusion, west Pilbara Block, Western Australia. *Economic Geology* **84**, 1775–1804.

Holzheid, A. & Lodders, K. (2001). Solubility of copper in silicate melts as function of oxygen and sulfur fugacities, temperature, and silicate composition. *Geochimica et Cosmochimica Acta* **65**, 1933–1951.

Ip, S. W. & Toguri, J. M. (1993). Surface and interfacial tension of the Ni–Fe–S, Ni–Cu–S, and fayalite slag systems. *Metallurgical Transactions* **24B**, 657–668.

Kress, V. C. & Carmichael, I. S. E. (1991) The compressibility of silicate liquids containing Fe_2O_3 and the effect of composition, temperature, oxygen fugacity and pressure on their redox states. *Contributions to Mineralogy and Petrology* **108**, 82–92.

Kucharski, M., Ip, S. W. & Toguri, J. M. (1994). The surface tension and density of Cu_2S, FeS, Ni_3S_2 and their mixtures. *Canadian Metallurgical Quarterly* **33**, 197–203.

LaTourrette, T., Wasserburg, G. J. & Fahey, A. J. (1996). Self diffusion of Mg, Ca, Ba, Nd, Yb, Ti, Zr, and U in haplobasaltic melt. *Geochimica et Cosmochimica Acta* **60**, 1329–1340.

Lesher, C. M. & Campbell, I. H. (1993). Geochemical and fluid dynamic modelling of compositional variations in Archean komatiite-hosted nickel sulfide ores in Western Australia. *Economic Geology* **88**, 804–816.

Lowry, R. K., Henderson, P. & Nolan, J. (1982). Tracer diffusion of some alkali, alkaline-earth and transition element ions in a basaltic and andesitic melt, and the implications concerning melt structure. *Contributions to Mineralogy and Petrology* **80**, 254–261.

Maier, W. D. & Barnes, S.-J. (1999). Platinum-group elements in silicate rocks of the Lower, Critical and Main Zones at Union Section, Western Bushveld Complex. *Journal of Petrology* **40**, 1647–1671.

Marsh, B. D. (1982). On the mechanics of igneous diapirism, stoping, and zone melting. *American Journal of Science* **282**, 808–855.

Mungall, J. E. (2002*a*). Empirical models relating viscosity and tracer diffusion in magmatic silicate melts. *Geochimica et Cosmochimica Acta* (in press).

Mungall, J. E. (2002*b*). Late-stage sulfide liquid mobility in the Main Mass of the Sudbury Igneous Complex; examples from the Victor Deep, McCreedy East and Trillabelle deposits. *Economic Geology* (in press).

Mungall, J. E., Dingwell, D. B. & Chaussidon, M. (1999). Chemical diffusivities of 18 trace elements in granitoid melts. *Geochimica et Cosmochimica Acta* **63**, 2599–2610.

Naldrett, A. J. & Wilson, A. H. (1990). Horizontal and vertical variations in noble-metal distribution in the Great Dyke of Zimbabwe: a model for the origin of the PGE mineralization by fractional segregation of sulfide. *Chemical Geology* **88**, 279–300.

Naldrett, A. J., Innes, D. G., Sowa, J. & Gorton, M. (1982). Compositional variation within and between five Sudbury ore deposits. *Economic Geology* **77**, 1519–1534.

Naldrett, A. J., Lightfoot, P. C., Fedorenko, V. A., Doherty, W. & Gorbachev, N. S. (1992). Geology and geochemistry of intrusions

and flood basalts of the Noril'sk region, USSR, with implications for the origin of the Ni–Cu ores. *Economic Geology* **87**, 975–1004.

Naldrett, A. J., Asif, M., Schandl, E., Searcy, T., Morrison, G. G., Binney, W. P. & Moore, C. (1999). Platinum-group elements in the Sudbury ores: significance with respect to the origin of different ore zones and to the exploration for Footwall ore bodies. *Economic Geology* **94**, 185–210.

O'Neill, H. St. C., Dingwell, D. B., Borisov, A., Spettel, B. & Palme, H. (1995). Experimental petrochemistry of some highly siderophile elements at high temperatures, and some implications for core formation and the Earth's early history. *Chemical Geology* **120**, 255–273.

Peach, C. L., Mathez, E. A. & Keays, R. R. (1990). Sulfide melt–silicate melt distribution coefficients for noble metals and other chalcophile elements as deduced from MORB: implications for partial melting. *Geochimica et Cosmochimica Acta* **54**, 3379–3389.

Pitts, D. R. & Sissom, L. E. (1977). *Heat Transfer*. Toronto, Ont.: McGraw–Hill.

Prendergast, M. D. (2000). Layering and precious metals mineralization in the Rinçon del Tigre Complex, Eastern Bolivia. *Economic Geology* **95**, 113–130.

Ripley, E. M. & Brophy, J. G. (1995). Solubility of copper in a sulphur-free mafic melt. *Geochimica et Cosmochimica Acta* **59**, 5027–5030.

Ryan, M. P. & Blevins, J. Y. K. (1987). *The Viscosity of Synthetic and Natural Silicate Melts and Glasses at High Temperatures and 1 Bar (105 Pascals) Pressure and at Higher Pressures. US Geological Survey Bulletin* **1764**.

Shannon, R. D. (1976). Revised effective ionic radii and systematic studies of interatomic distances in halides and chalcogenides. *Acta Crystallographica* **A32**, 751–767.

Shaw, H. R. (1972). Viscosities of magmatic silicate liquids: an empirical method of prediction. *American Journal of Science* **272**, 870–893.

Toplis, M. J. & Carroll, M. R. (1995). An experimental study of the influence of oxygen fugacity on Fe–Ti oxide stability, phase relations, and mineral–melt equilibria in ferro-basaltic systems. *Journal of Petrology* **36**, 1137–1170.

von Gruenewaldt, G., Sharpe, M. R. & Hatton, C. J. (1985). The Bushveld Complex: introduction and review. *Economic Geology* **80**, 803–812.

Watson, E. B. (1994). Diffusion in volatile-bearing magmas. In: Carroll, M. R. & Holloway, J. R. (eds) *Volatiles in Magmas. Mineralogical Society of America, Reviews in Mineralogy* **30**, 371–411.

Wendlandt, R.F. (1982). Sulfide saturation of basalt and andesite melts at high pressures and temperatures. *American Mineralogist* **67**, 877–885.

Williams, D. A., Kerr, R. C. & Lesher, C. M. (1999). Thermal and fluid dynamics of komatiitic lavas associated with magmatic Fe–Ni–Cu–(PGE) deposits. In: *Dynamic Processes in Magmatic Ore Deposits and their Application in Mineral Exploration. Geological Society of Canada Short Course Notes* **13**, 367–412.

Wilson, A. H. & Tredoux, M. (1990). Lateral and vertical distribution of platinum-group elements and petrogenetic controls on the sulfide mineralization in the P1 pyroxenite layer of the Darwendale subchamber of the Great Dyke, Zimbabwe. *Economic Geology* **85**, 556–584.

APPENDIX: DERIVATION OF EQUATIONS GOVERNING MASS TRANSFER

Static spherical droplet

The diffusion problem will be considered in a static radial coordinate system, described as follows (Crank, 1975):

$$C_{(r,t)} = C_o + \frac{a}{r}(C_s - C_o)\left(1 - \mathrm{erf}\left\{\frac{r-a}{\sqrt{4Dt}}\right\}\right) \quad \text{(A1)}$$

where $C_{(r,t)}$ is the concentration of the metal in the silicate melt at a distance r from the interface at time t, C_o is the initial concentration of the metal throughout the silicate melt, and C_s is the concentration of the metal in the silicate melt at the interface. The diffusivity of the metal in the silicate melt is D, a is the radius of the sulfide droplet, and erf$\{x\}$ is the error function, which is defined as (e.g. Gautschi, 1972)

$$\mathrm{erf}\{x\} = \frac{2}{\sqrt{\pi}}\int_0^x \exp\{-n^2\}\,\mathrm{d}n. \quad \text{(A2)}$$

The choice of a static model for what is in reality a moving boundary problem is driven by the difficulty of working with moving boundaries in spherical coordinates, and justified by the assumption that the rate of growth of the sulfide body will be negligible because it is being fed by chemical components that are all trace elements in the host silicate melt. The flux of the metal at a given radius r is given by Fick's first law

$$\mathcal{J} = -\rho_{sil} D\frac{\partial C}{\partial r} \quad \text{(A3)}$$

where ρ_{sil} is the density of the silicate melt. Substituting equation (A1) into equation (A3) and evaluating at the interface where $r = a$ gives the flux of metal into the droplet as a function of time:

$$\mathcal{J} = -\rho_{sil}(C_o - C_s)\left(\frac{D}{a} + \sqrt{\frac{D}{\pi t}}\right). \quad \text{(A4)}$$

Integration of equation (A4) with respect to time gives the amount M of the metal of interest that will have passed through a given area of interface in a given time:

$$M = -\rho_{sil}(C_o - C_s)\left(\frac{Dt}{a} + \sqrt{\frac{4Dt}{\pi}}\right). \quad \text{(A5)}$$

Static planar interface

The solution to the diffusion equation for a one-dimensional flux into a half-space is

$$C_{(x,t)} = C_s + (C_o - C_s)\frac{2}{\sqrt{\pi}}\mathrm{erf}\left\{\frac{x}{\sqrt{aDt}}\right\} \quad \text{(A6)}$$

where $C_{(x,t)}$ is the concentration of the metal in the silicate melt at a distance x from the interface at time t, and the other variables are as in equation (A1).

Substituting again into equation (A3) and evaluating at the interface where $x = 0$, we find that

$$\mathcal{J} = -\rho_{sil}(C_o - C_s)\sqrt{\frac{D}{\pi t}} \quad \text{(A7)}$$

which can also be obtained from equation (A4) by setting $a = \infty$. Taking the time integral of (A10) as before we obtain the mass flux per unit area into the sulfide pool:

$$M = -\rho_{sil}(C_o - C_s)\sqrt{\frac{4Dt}{\pi}}. \quad \text{(A8)}$$

Convective mass transfer: moving silicate melt above a planar interface

An important dimensionless quantity in heat and mass transfer is the Reynold's number Re, defined as

$$\mathrm{Re} = \frac{vL\rho_{sil}}{\eta} \quad \text{(A9)}$$

where v is the velocity of a flow, L is the characteristic distance over which the flow is felt, ρ_{sil} is the density of the silicate melt, and η is the dynamic viscosity of the silicate melt. The Reynolds number expresses the ratio between the inertial and viscous forces in a flow; flows with Re greater than several thousand tend to be turbulent, whereas low Reynolds number flows are laminar.

Several other dimensionless numbers are commonly used in the description of heat transfer. By taking appropriate transformations one can find compositional analogs. I begin by defining a mass transfer coefficient m through the following equation, which is analogous to Newton's law of heat transfer:

$$\mathcal{J} = m(C_o - C_s) \quad \text{(A10)}$$

where $\mathcal{J}$, C_o and C_s are defined as before. The mass transfer coefficient in (A10) has units of flux (mass per unit area per second) and depends upon the concentration gradient and width of the diffusion region. It is not a constant, but relates the measureable flux to the magnitude of the concentration difference between interface and far field. Using the mass transfer coefficient I define a compositional Nusselt number Nu*, which expresses the ratio between convective and diffusive length scales:

$$\mathrm{Nu}^* = \frac{mL}{D\rho_{sil}} \quad \text{(A11)}$$

where L is a characteristic length (e.g. radius of a spherical drop) and D and ρ_{sil} are as defined above. The compositional Prandtl number Pr*, defined as

$$\mathrm{Pr}^* = \frac{\eta}{\rho D} \quad \text{(A12)}$$

relates the scale of the velocity field to the scale of the diffusion region. Systems with high Prandtl number are dominated by diffusive fluxes, whereas low Prandtl number leads to dominant convective fluxes. Finally, the compositional Peclet number Pe* is defined as the product of the Reynolds and compositional Prandtl numbers, giving it the following form:

$$\mathrm{Pe}^* = \frac{vL}{D} \quad \text{(A13)}$$

the Peclet number indicates the ratio between the amounts of mass transfer effected by convection and diffusion.

The extremely low viscosity of sulfide liquids allows their interfaces with silicate melts to be treated as free-slip boundaries. Consequently, the flow of silicate melt past a pool of effectively zero viscosity can be treated as ideal slug flow in which there is no velocity gradient. In the case of the spherical droplet suspended in the silicate melt, the fall velocity estimated using Stokes' law must be adjusted because the drag on a falling droplet is diminished by two-thirds if the drop is inviscid (e.g. Marsh, 1982).

I first consider a body of silicate melt moving with a velocity v in the direction x above a sulfide pool with a depth a and a downstream extent X, the two bodies being separated by a planar interface. Pitts & Sissom (1977, p. 175) compared empirical measurements and approximate solutions to a similar heat flow problem; the corresponding expression for the instantaneous mass transfer coefficient is

$$m = \frac{3\sqrt{2}}{8}\rho_{sil}\sqrt{\frac{Dv}{y}} \quad \text{(A14)}$$

where m varies with position y because the efficiency of the transfer is greatest at the leading edge of the pool where the fresh undepleted melt first encounters the sulfides. I find an average mass transfer coefficient for the pool as a whole, by taking the integral of equation (A14) with respect to y over the length of the pool and dividing by X; this is substituted into equation (A10) to give the flux into the pool as a function of pool size:

$$\mathcal{J} = \frac{3\sqrt{2}}{4}(C_o - C_s)\rho_{sil}\sqrt{\frac{Dv}{X}}. \quad \text{(A15)}$$

Integrating $\mathcal{J}$ with respect to time gives the time-dependent mass flux M into the pool:

$$M = \frac{3\sqrt{2}}{4}(C_o - C_s)\rho_{sil}\sqrt{\frac{Dt^2v}{X}}. \quad \text{(A16)}$$

Convective mass transfer: moving spherical droplet

The case of the spherical droplet can be treated by using the dimensionless parameters that characterize the flow

and the diffusive process as described above. The way forward is to estimate the flux $\mathcal{J}$ by combining equations (A10) and (A11) through their common dependence on the mass transfer coefficient;

$$\mathcal{J} = \frac{\mathrm{Nu}^* D\rho_{\mathrm{sil}} (C_\mathrm{o} - C_\mathrm{s})}{L}. \qquad \text{(A17)}$$

The Nusselt number can be expressed as a function of the Peclet number for liquid spheres moving through a viscous fluid at high Prandtl number, by using an approximation proposed by Marsh (1982):

$$\mathrm{Nu}^* = 1 + \frac{1}{2}\mathrm{Pe}^{*\,\frac{1}{2}}. \qquad \text{(A18)}$$

Equation (A18) reproduces Nu* moderately well where it is known analytically, and is the only available means of estimating Nu* for $1 < \mathrm{Pe}^* < 10$. Applying the definition of Pe*, the flux can be estimated as

$$\mathcal{J} = \frac{D\rho_{\mathrm{sil}} (C_\mathrm{o} - C_\mathrm{s})}{L}\left[1 + \frac{1}{2}\left(\frac{vL}{D}\right)^{\frac{1}{2}}\right]. \qquad \text{(A19)}$$

Two possibilities present themselves for the evaluation of equation (A19). In one case, the sulfide droplet can be considered to be moving through a static silicate melt by Stokes' flow. The Stokes' equation for velocity of an inviscid sphere falling in a viscous fluid is

$$v = \frac{2\Delta\rho g a^2}{\eta} \qquad \text{(A20)}$$

where v is the fall velocity of the droplet, $\Delta\rho$ is the difference in density between the silicate and sulfide melts, and g is the acceleration due to gravity. Setting $L = a$ gives

$$\mathcal{J} = \rho_{\mathrm{sil}} (C_\mathrm{o} - C_\mathrm{s})\left(\frac{D}{a} + \sqrt{\frac{Dv}{4a}}\right). \qquad \text{(A21)}$$

Taking the integral with respect to time as before to find M, the amount of metal passing through a unit area in a given time, leads to

$$M = t\rho (C_\mathrm{o} - C_\mathrm{s})\left(\frac{D}{a} + \sqrt{\frac{Dv}{4a}}\right). \qquad \text{(A22)}$$

If the velocity imposed by an external flow is much greater than the velocity resulting from the density difference of the two liquids in the gravity field, then the Stokes' flow velocity is negligible. The velocity of the flow in the vicinity of the droplet can be obtained by first finding the average velocity gradient of the flow, equal to the velocity difference between the interior of the flow and a no-slip boundary divided by the distance across the viscous boundary layer. An effective velocity can be estimated by multiplying the velocity gradient by the characteristic length of the droplet, taken here to be its radius a, leading to

$$M = t\rho (C_\mathrm{o} - C_\mathrm{s})\left(\frac{D}{a} + \sqrt{\frac{Dv}{4L}}\right). \qquad \text{(A23)}$$